Electrocatalysis of hydrogen and oxygen electrode reactions in alkaline media by Rh-modified polycrystalline Ni electrode

Ljubinka Vasić[1], Nikola Tričković[1], Zaharije Bošković[1], Aleksandar Z. Jovanović[1], Natalia V. Skorodumova[2,3], Slavko V. Mentus[1,4], Igor A. Pašti[1]

[1] *University of Belgrade – Faculty of Physical Chemistry, Studentski trg 12-16, 11000 Belgrade, Serbia*

[2] *Department of Materials Science and Engineering, School of Industrial Engineering and Management, KTH – Royal Institute of Technology, Brinellvägen 23, 100 44 Stockholm, Sweden*

[3] *Applied Physics, Division of Materials Science, Department of Engineering Sciences and Mathematics, Luleå University of Technology, 971 87 Luleå, Sweden*

[4] *Serbian Academy of Sciences and Arts, Kneza Mihaila 35, 11000 Belgrade, Serbia*

Corresponding author

Prof. Dr. Igor A. Pašti

University of Belgrade – Faculty of Physical Chemistry

E-mail: igor@ffh.bg.ac.rs

Abstract

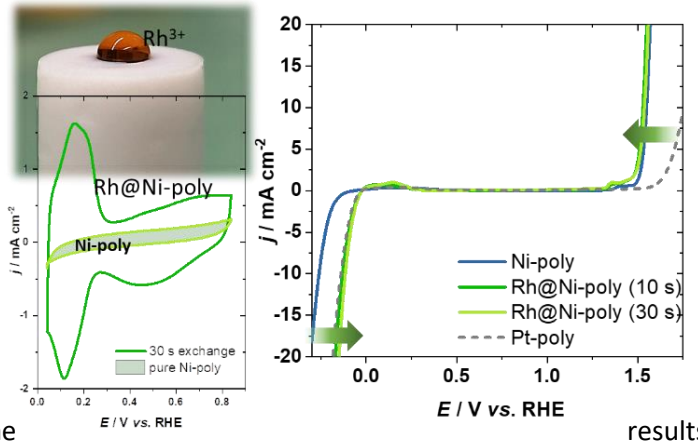

Developing novel electrocatalysts for energy conversion applications is of utmost importance for reaching the energy security of modern society. Here we present a comprehensive investigation of rhodium-modified polycrystalline nickel as an electrocatalyst for hydrogen and oxygen electrode reactions in alkaline media. The surface modification of nickel electrodes was achieved by facile galvanic displacement (up to 30 seconds) from a highly concentrated acidic Rh^{3+} solution. The results demonstrate a significant enhancement in the electrocatalytic activity for both hydrogen evolution reaction (HER) and oxygen evolution reaction (OER) on the Rh-modified Ni electrodes, positioning galvanic displacement as a viable approach to engineering advanced electrocatalysts for clean energy applications. On the other hand, the hydrogen oxidation (HOR) and oxygen reduction reaction (ORR) activities of the Rh-modified electrodes are lower compared to polycrystalline platinum. It is suggested that semiconducting Rh_2O_3 has a detrimental role on the HOR and ORR performance, while the activities of HER and OER, dominantly taking place on metallic Rh and conductive RhO_2, are very high. This research sheds light on the mechanisms underlying the enhanced electrode kinetics on Rh-modified Ni electrodes and provides insights into the development of efficient and cost-effective electrocatalysts for renewable energy technologies.

Keywords: galvanic displacement; nickel; rhodium; electrocatalysis; water splitting.

1. Introduction

Electrochemical energy conversion is a critical pillar of modern society, profoundly impacting our daily lives and the global energy landscape [1,2]. From powering portable devices like smartphones and laptops to driving the sustainable transportation revolution through electric vehicles, electrochemical energy conversion has become indispensable. It enables the integration and storage of renewable energy sources, fostering a cleaner and greener future.

The hydrogen economy is centered around the crucial interplay of water splitting and fuel cell technologies, offering a promising pathway towards a more sustainable and clean energy future [3,4]. Water splitting, especially through electrolysis, plays a fundamental role in this vision by generating hydrogen from water using renewable energy sources like solar and wind power [5–8]. This process yields "green hydrogen," which can be stored, transported, and utilized as a versatile energy carrier across diverse industries and applications [9]. Fuel cell technologies complement the hydrogen economy by providing a clean and efficient method to convert hydrogen and oxygen into electricity [10–12]. The hydrogen economy holds transformative potential in various sectors, offering opportunities to reduce carbon emissions, enhance energy security, and foster a cleaner, more resilient energy landscape. As research and development continues and infrastructure for hydrogen production, distribution, and utilization advances, the hydrogen economy is poised to play a pivotal role in achieving a sustainable and low-carbon future.

The hydrogen and oxygen electrode reactions play crucial roles when it comes to water splitting and fuel cell technologies. Hydrogen evolution/oxidation reactions (HER/HOR) can be summarized as:

$$2H^+ + 2e^- = H_{2(g)} \quad (1)$$

in alkaline media, and:

$$2H_2O + 2e^- = H_{2(g)} + 2OH^- \quad (2)$$

in acidic media. Analogously, oxygen evolution/reduction reactions (OER/ORR) can be presented as:

$$O_{2(g)} + 4H^+ + 4e^- = 2H_2O \quad (3)$$

in alkaline media, and:

$$O_{2(g)} + 2H_2O + 4e^- = 4OH^- \quad (4)$$

in acidic media. While HER and OER take place in water electrolysis systems, HOR and ORR occur in the fuel cell anode and cathode, respectively. However, proper electrocatalysts are needed in order to proceed with any of these reactions. In acidic media, catalyst corrosion is very prominent; thus, noble metal catalysts are used. On the other hand, in alkaline media, non-noble materials are used because the corrosion is less pronounced. In practice, nickel and nickel-based electrocatalysts are most commonly used in alkaline media [13]. The catalytic activity of pure nickel can be tuned by morphology and the active surface area [14,15]. Further strategies to improve the catalytic activity of Ni are alloying with noble [16,17] and non-noble metals, like Mo [18], Cu [19], and Co [20]. Additionally, the interfacial effects could enhance H_2 production via improved water splitting [21] or the facilitated recombination of adsorbed hydrogen intermediates into H_2 [22,23].

Due to suitable adsorption energetics of HER/HOR and OER/ORR reaction intermediates, platinum group metals usually exhibit very high catalytic activities [24,25], although no single metal is an excellent catalyst for all four reactions. Typically, platinum and iridium stand out as benchmark catalysts for these reactions [26]. Moreover, not only do the activities of noble and platinum group metals towards hydrogen and oxygen electrode reactions vary, but their prices differ to a great extent and are quite volatile [27], making any solid predictions about their widespread usage quite difficult. Thus, an understanding of the

fundamental properties of different noble metal-based catalysts is needed as the potential for their wider application can open easily due to price variations combined with high catalytic activities.

Rhodium is usually considered an extremely pricy metal, but its price is currently below that of iridium [27]. As demonstrated, to significantly contribute to the catalysis of hydrogen and oxygen electrode reactions [28–32], further investigation of Rh-containing electrocatalysts is needed. In particular, the catalysts where only the surface layer is modified with small amounts of Rh could be especially attractive due to a low penalty in terms of the catalyst price. In our previous work, we have shown that Ni can be modified by small amounts of Rh by galvanic displacement according to the reaction $3Ni_{(s)} + 2Rh^{3+} = 3Ni^{2+} + 2Rh_{(s)}$ [33]. When this reaction is performed in a highly acidic and concentrated Rh salt solution, it takes under one minute to significantly boost the HER activity of flat nickel surfaces and several minutes to improve the activity of nickel foam and electrodeposited nickel layers. The same approach works for polycrystalline cobalt electrodes and, besides HER, significantly improves OER [34].

In this work, we have conducted surface modification of a polycrystalline nickel (Ni) electrode through galvanic displacement using rhodium (Rh), following the approach described in our previous works [33,34]. The electrocatalytic activity of the modified Ni electrode for the HER/HOR and OER/ORR was thoroughly examined using electrochemical techniques and compared to that of unmodified Ni electrodes and polycrystalline platinum. The results demonstrate a substantial enhancement in the electrode reactions' efficiency on the Rh-modified Ni surface, showcasing the potential of galvanic displacement as a promising strategy for engineering advanced electrocatalysts with applications in clean energy technologies.

2. Experimental

2.1. Electrode preparation

All the measurements were done using smooth polycrystalline Ni (Ni-poly) rotating disk electrodes (RDE). The Ni disk had a diameter of 3.2 mm and was inserted in a Teflon cylinder with a 10 mm diameter. The Ni disk was made of Ni rod (Goodfellow Cambridge Limited, England, 99.9 %). Before the modification with Rh, the disk was polished with alumina-based grinding paper, sonicated for 1 minute, washed in deionized water, subsequently in diluted HCl, and again in deionized water. Galvanic displacement was done by drop-casting 10 µL of 0.1 mol dm^{-3} $RhCl_3$ (Sigma Aldrich) solution in 0.1 mol dm^{-3} $HClO_4$ for a specified amount of time (up to 303 s). After the exchange, the electrode was rinsed in deionized water, then in 0.1 mol dm^{-3} KOH or 1 mol dm^{-3} KOH solution, covered with the droplet of the same solution, and quickly transferred into the electrochemical cell. The transfer to the cell typically took under 30 s. For the measurements of clean Ni-poly, the electrode was transferred to the electrochemical cell directly after the polishing. The roughness factor (RF) [35] of such prepared Ni-poly electrodes amounts to 10±1, determined by double-layer capacitance measurements as described in [33].

As a benchmark, we used a platinized Pt-poly disk (3 mm in diameter, Goodfellow Cambridge Limited, England, 99.9 %), prepared by potentiodynamic cycling of a smooth Pt-poly disk in H_2PtCl_6 solution, as described in ref. [36]. Two Pt-poly electrodes were prepared with RF amounting to 5 and 20 (determined using H_{UPD} peaks). HER/OER and HOR/ORR activities of Pt-poly electrodes were measured in the same way as for the Ni-poly and Rh-modified Ni-poly electrodes.

Morphology analysis and surface chemical composition were probed using SEM-EDX with Phenom ProX Scanning Electron Microscope (Phenom, Netherlands). SEM characterization was done using an acceleration voltage of 10 kV, while the chemical composition was probed with an acceleration voltage of 15 kV. Characterization was done without the deposition of a conductive layer on the electrodes.

2.2. HER/OER measurements

HER and OER activity of Ni and Rh-modified electrodes was measured using a specific protocol, which was started immediately after the electrode transfer to the electrochemical cell. The program for the HER and OER activity measurements was constructed in such a way as to avoid undesirable anodic excursions of studied electrodes or any equilibration at the open circuit potential (OCP). For all the measurements IVIUM Vetex.One potentiostat was used. Measurements were done in a one-compartment, three-electrode electrochemical cell with a Saturated Calomel Electrode (SCE) as a reference electrode and a 3×3 cm Ni foam (Goodfellow Cambridge Limited, England) as a counter electrode. The electrolytic solutions were prepared using KOH (Sigma Aldrich) and ultrapure deionized water. All the measurements were done at room temperature. Here, the potentials are referred to as the Reversible Hydrogen Electrode (RHE) scale by directly measuring the potential of the used reference SCE electrode *versus* the RHE formed in the corresponding electrolytic solutions. Electrolyte resistance was corrected using hardware settings, but only to 70 % of the resistance value. The electrolyte resistance was determined using single-point impedance measurement at −1 V *vs*. SCE (approx. 0 V vs. RHE). The gasses used in this study were of 99.999 % purity.

The protocol for the measurements consisted of deep cathodic sweeps for accessing HER activity (three cycles at 20 mV s^{-1} between 0 and −0.35 V *vs*. RHE) separated by electrode cycling to progressively higher anodic potential (three cycles at 50 mV s^{-1} between 0 and 0.8, 1.0, and 1.2 V *vs*. RHE). HER overpotentials were estimated from the anodic part of the third cycle. This part of the protocol ended with three wide cyclic voltammograms (50 mV s^{-1} between 0 and 1.45 V *vs*. RHE), after which one cycle between −0.35 and 1.65 V *vs*. RHE was done (at 20 mV s^{-1}). During the HER measurements and the last cyclic voltammogram, the electrode was rotated at 1800 rpm in order to remove any H_2 or O_2 bubbles formed on the surface, which could block the electrode surface.

2.3. HOR/ORR measurements

For Rh-modified Ni-poly, HOR measurements were done immediately after the galvanic displacement and after 25 cycles between 0 and 1.2 V vs. RHE, i.e., electrochemical cleaning of the electrode surface. Measurements were done in H_2-saturated 0.1 mol dm^{-3} solution using the RDE technique, and the potential sweep rate was 10 mV s^{-1}. After the HOR measurements, the electrolyte was purged with N_2, and the electrode was extensively cycled. When a stable cyclic voltammogram was obtained, the blank cyclic voltammogram (background) was recorded between 0.05 and 1.0 V *vs*. RHE. Then, the electrolyte was saturated with O_2, and the ORR polarization curves were recorded using the RDE technique. The potential sweep rate was 20 mV s^{-1}.

2.4. DFT calculations

The first-principle DFT calculations were performed using the Vienna ab initio simulation code (VASP) [37,38]. The Generalized Gradient Approximation (GGA) in the parametrization by Perdew, Burk, and Ernzerhof [39] combined with the projector augmented wave (PAW) method was used [40]. A cut-off energy of 520 eV was used, while the Monkhorst–Pack *Γ*-centered 5×5×8 k-point mesh was used for tetragonal RhO_2, and 4×4×3 k-point mesh was set for orthorhombic Rh_2O_3. For Density of States calculations, partial occupancies were treated using the tetrahedron method with Blöchl correction [41].

3. Results and Discussion

3.1. Rh-modified Ni electrodes

Here we first confirm the successful deposition of Rh on the Ni-poly electrode. The exchange was done for 10 and 30 seconds, as we have previously shown that longer deposition times for smooth Ni electrodes do not enhance further HER activity. However, previously we have not observed Rh H_{UPD} peaks [42] for 10 s exchange (mirror-finish polished Ni-poly), while here could clearly observe these features in cyclic voltammogram (**Figure 1**, a).

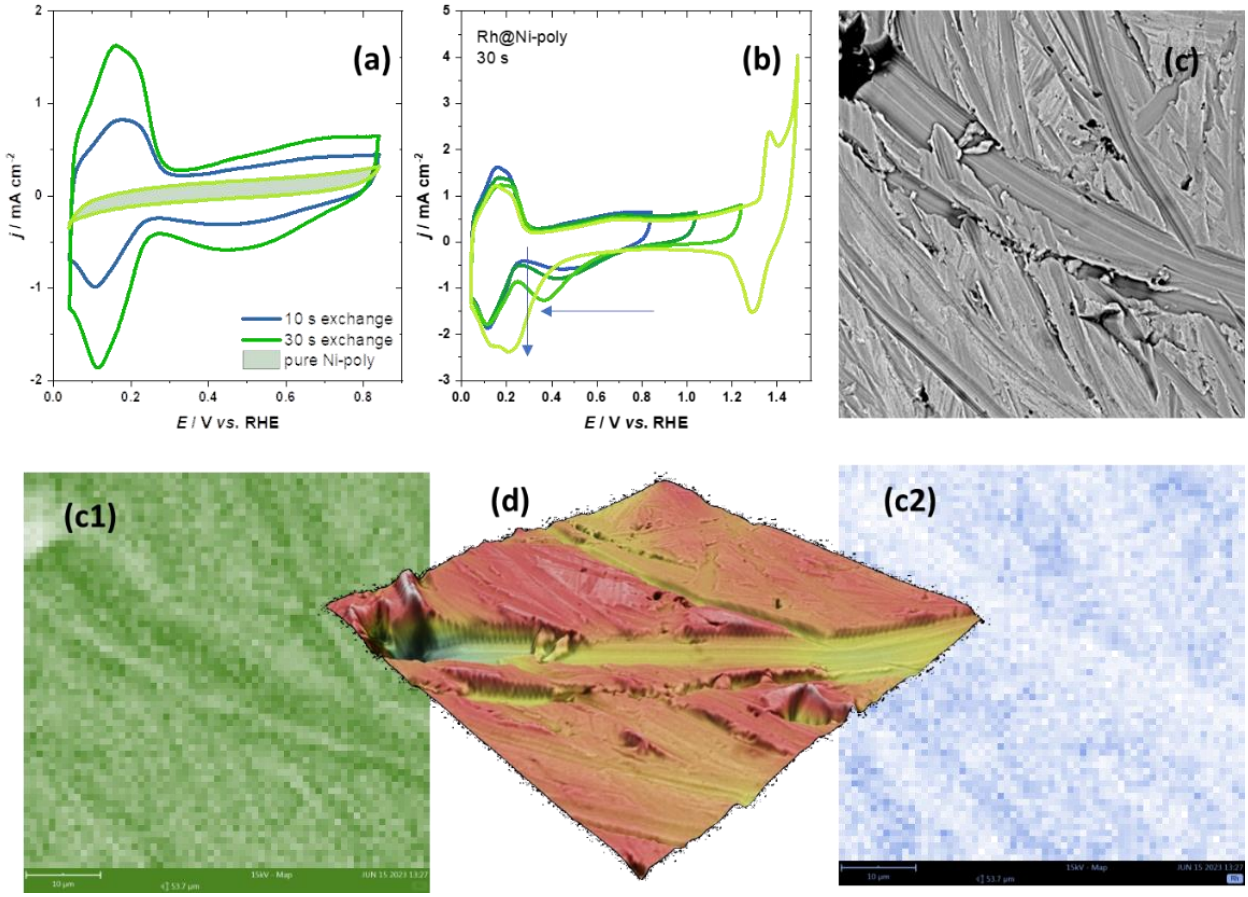

Figure 1. (a) cyclic voltammograms of pure Ni-poly and Rh-modified Ni-poly electrodes (50 mV s^{-1}, N_2 purged 1 mol dm^{-1} KOH); (b) successive cyclic voltammograms of Rh-modified Ni-poly electrode with increasing anodic vertex; (c) SEM image of the Rh-modified electrode (30 s of exchange, ×5,000 magnification) with the corresponding Ni map (c1) and Rh map (c2), confirming Rh deposition on the Ni electrode surface; (d) 3D SEM reconstruction of the same spot.

Upon extending the deposition time to 30 seconds, the peaks roughly double in size and become more prominent. The cycling of the electrode to progressively higher anodic potentials (**Figure 1**, b) reveals that the main surface electrochemistry of Rh is well-separated from the main features of Ni electrochemistry (**Figure 1**, b), also suggesting that after 30 s of galvanic exchange, the Ni-poly surface is only partially covered with Rh. Besides the already mentioned H_{UPD} peaks of Rh (0.05 to 0.3 V vs. RHE), the oxidation of the Rh phase takes place already at E > 0.4 V vs. RHE. Similarly to other noble metals, like Pt [43], the oxidation and reduction of the Rh phase are characterized by pronounced irreversibility, and for the case of Rh, we observe an extreme behavior. Namely, as the anodic vertex goes deeper into the anodic direction, the reduction of Rh oxide shifts to progressively more negative potentials. When the electrode

is cycled up to 1.45 V vs. RHE, the reduction of Rh oxide shifts to very negative potentials, practically overlapping with the H_{UPD} region. This could also explain the smaller anodic peak of H_{UPD} upon progressively deeper anodic excursions of Rh-modified Ni-poly. One logical assumption would be that Rh is lost from the surface layer, as it is known that there is anodic dissolution of Rh upon anodic excursions [44]. However, the Rh dissolution rate at high anodic potentials (corresponding to OER conditions) in alkaline media is lower compared to Ru and Ir, and slightly higher compared to that of Pt and Pd. On the other hand, under potential cycling, the Rh dissolution rate is the lowest among the metals considered by Schalenbach et al. [44] (Ag, Au, Ir, Pd, Pt, Rh, and Ru). Thus, the reduction of the anodic H_{UPD} peak can be ascribed to the cathodic contribution of hardly reducible Rh oxide reduction upon anodic excursions.

We note that the electrode surface is relatively rough, which is the result of the electrode polishing by grinding paper. 3D SEM reconstruction shows roughness around 1 µm, while EDX analysis revealed under 2 at. % of Rh on the surface, with an additional ~4 at. % of oxygen (**Figure 1**, c and d). These results agree with the previous EDX measurements on smooth Rh-modified Ni-poly [33]. In the same work, XPS measurements revealed between 12.5 and 60 at. % of Rh, as the modification is restricted to the surface layer, at least half of it coming from the metallic Rh phase. For 45 seconds of exchange, we were previously able to observe Rh nanoparticles on the surface, but the overall amount of Rh was very small, so XRD was not able to detect the Rh phase even upon prolonged exchange on Ni foam electrode [33].

3.2. Water splitting in alkaline media – HER and OER electrocatalysis

HER activity of Ni-poly was significantly improved upon the surface modification by Rh (**Figure 2**). The activity of as-prepared electrodes increases in the order Ni-poly < Rh-modified Ni-poly (10 seconds) < Rh-modified Ni-poly (30 seconds). Here we have systematically addressed the effects of surface oxidation of the studied electrodes to obtain deeper insight into the HER mechanism. For pure Ni-poly, surface oxidation causes a progressive increase in activity. Here, the oxidation was performed by potential cycling to increasingly higher anodic potentials as explained. For Ni-poly, the activity (measured as overpotential needed to reach −10 mA cm^{-2} [26], here denoted $\eta_{HER,10}$) increased for the potentiodynamic oxidation up to 1.2 V vs. RHE and then dropped slightly when the electrode was exposed to high anodic potentials of 1.45 V vs. RHE (**Table 1**).

Such an activity improvement can be understood by the formation of oxidized domains on the Ni surface, which boosts HER activity in alkaline media by speeding up water dissociation at the oxide|metal interface [21,45,46]. Recently it was shown that such potentiodynamic oxidation of Ni does not lead to surface roughening while increasing the HER exchange current densities 3-5 times [47]. Still, the HER activity of oxidized Ni electrodes is very far from that of Pt (**Figure 2**, top row – pure Ni-poly). We also note that here we have observed rather high ORR activity of the Ni-poly electrode (consistently over five repeated measurement sets), with η_{OER} significantly lower compared to the previously reported value by McCrory et al., amounting to 0.46 V, which might be due to the lower roughness factor of Ni electrode in that particular work (RF = 2) [26]. Also, we note that previously high OER activity of pure Rh electrode was reported, with the onset around 1.6 V vs. RHE (overpotential above 0.35 V), and it was also shown to be much more active than Pt (OER onset potential around 1.7 V vs. RHE) [44].

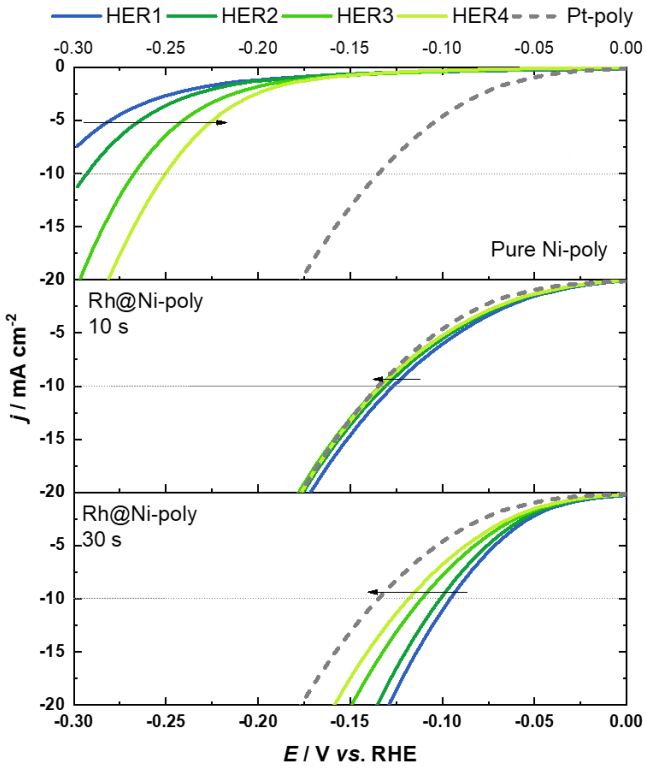

Figure 2. HER polarization curves (10 mV s^{-1}, N_2 purged 1 mol dm^{-1} KOH) of pure Ni-poly, and Rh-modified Ni-poly for 10 s of exchanges (middle panel) and 30 s of exchange (lower panel), as-prepared (HER1) and upon successive oxidation to 0.8 V vs. RHE (HER2), 1.0 V vs. RHE (HER2), and 1.2 V vs. RHE (HER3). Pt-poly (RF = 5) is added as a benchmark (dashed line). Arrows indicate the change in the activity trends.

Table 1. Summary of HER/OER catalysis (uncertainties of individual measurements are < 10 mV; thus, for example, all the overpotentials for HER on the Rh-modified Ni-poly with 10 s exchange are rounded to −0.13 V).

Electrode		**HER activity** $\eta_{HER,10}$ **/ V**	**OER activity** $\eta_{OER,10}$ **/ V**
Ni-poly	**As-prepared**	< −0.30	0.32
	Oxidized 1	−0.29	
	Oxidized 2	−0.27	
	Oxidized 3	−0.25	
	Oxidized 4[a]	−0.26	
Rh@Ni-poly (10 seconds)	**As-prepared**	−0.13	0.30
	Oxidized 1	−0.13	
	Oxidized 2	−0.13	
	Oxidized 3	−0.13	
	Oxidized 4 [a]	−0.13	
Rh@Ni-poly (20 seconds)	**As-prepared**	−0.09	0.31
	Oxidized 1	−0.10	
	Oxidized 2	−0.11	
	Oxidized 3	−0.12	
	Oxidized 4 [a]	−0.12	

Pt-poly (RF = 5)	−0.14	0.52
Pt-poly (RF = 20)	−0.11	0.51
Pt (RF = 10) [b]	−0.10±0.02	
Pt (RF = 130) [b]	−0.03±0.02	
Ru (RF = 70) [b]		0.29±0.02
Ru (RF = 200) [b]		0.34±0.03

[a] after a wide cyclic voltammogram up to 1.45 V vs. RHE, [b] Ref. [26], 1 mol dm^{-3} NaOH

For the Rh-modified electrodes, the situation is quite complex. First, the activities of the modified electrodes are close to or higher than that of platinized Pt, used here as benchmarks (**Figure 2**), or previously reported in the literature [26] (**Table 1**). HER activity is higher for longer surface modification time (30 s). However, the effects of surface oxidation are different for two Rh exchange times. For 10 seconds exchange, the activity drops, but only slightly, and all the overpotentials are within 10 mV (Table 1). In contrast, in the case of 30 seconds of exchange, the HER activity decays more but still remains higher than the activity Pt-poly (**Figure 2**, row – Rh@Ni-poly 30 s). Previously we have discussed similar effects induced by potentiostatic oxidation of Rh-modified Ni-poly electrode [33], suggesting that the oxidized phase of Rh-Ni could be less effective for H_2O dissociation compared to the as-prepared Rh-Ni phase. Moreover, it was shown that the Rh-Ni phase offers better H_{ads} energetics compared to the Ni surface. Here we see that the activity increases with the amount of Rh deposited on the electrode, but the effects of surface oxidation are also more prominent in that case. Thus, Ni|Rh interface could be the key for a high HER activity, while Rh sites could serve as H_{ads} acceptors where the H_2 formation is taking place, as the Rh surfaces provide much better H_{ads} energetics than Ni surfaces. However, the influence of oxides could be present even in the case of pure Rh phase, as previously shown [48], suggesting that the kinetics of Rh oxide reduction has a significant impact on the catalytic activity.

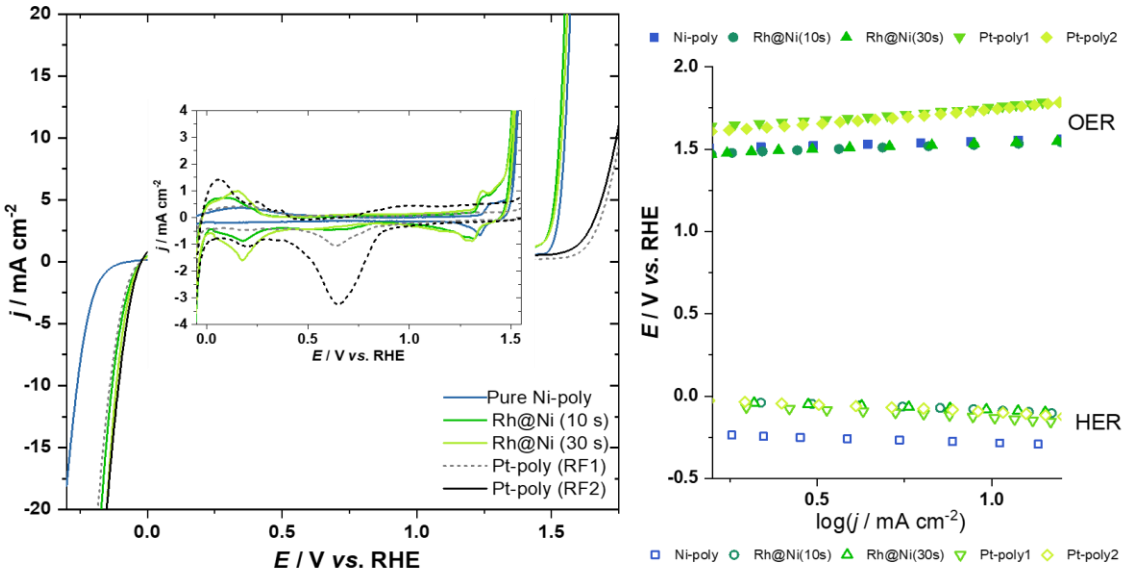

Figure 3. HER/OER polarization curves studied electrodes (10 mV s^{-1}, N_2 purged 1 mol dm^{-1} KOH), from pure Ni-poly to Rh-modified Ni-poly and benchmark Pt electrode (RF1 = 5, RF2 = 20), inset provides magnified cyclic voltammogram of the studied electrodes in the 0-1.5 V vs. RHE range (left), HER and OER Tafel plots of the corresponding electrodes.

After exposing the electrodes to high anodic potentials (1.45 V vs. RHE), a wide cyclic voltammogram was recorded to probe HER and OER activity, that is to determine the overall water-[48]splitting voltage on the studied electrodes (**Figure 3**, left). The cycle started in the cathodic direction, thus, HER was probed first, and then OER was tested. Overpotentials for HER ($\eta_{HER,10}$, **Table 1**, oxidation4) and OER ($\eta_{OER,10}$, **Table 1**) were extracted from this cyclic voltammogram. Further, Tafel slopes were evaluated (**Table 2**). To evaluate Tafel slopes, a single current decade, from |2| to |20| mA cm^{-2} was fitted using a linear fit (**Figure 3**, right). In this way, both HER and OER overpotentials were high enough for the fitting, while gas bubbles formation was not as high to cause partial electrode surface blockage.

As can be seen, Pt-poly has a low HER overpotential and a high OER overpotential, while pure Ni-poly behaves the opposite, with a high HER overpotential and lower OER overpotential. However, Rh-modified Ni-poly combines both low HER overpotential and low OER overpotential, while it is also characterized by low values of HER and OER Tafel slopes (**Table 2**). Considering the OER catalyst overview provided by Plevová et al. [49], the Rh-modified Ni-poly electrodes fall in the high activity group of OER electrocatalysts presented so far, surpassing more than 70% of them. The values of HER and OER overpotentials, together with the calculated Tafel slopes, were used to estimate water decomposition voltage at 1000 mA cm^{-2} (**Table 2**, $U_{iR\text{-free}}$). We note that these are iR-free water decomposition voltages to the extent to which we were able to remove iR drop from the cyclic voltammograms presented in **Figure 3** (left). Based on the obtained results, the Rh-modified Ni-poly electrodes offer water decomposition voltages below 2 V at a high current density of 1000 mA cm^{-2} (geometric), which is 20% lower compared to the water decomposition voltage on pure Ni electrodes estimated here.

Table 2. Tafel slopes for HER and OER (fitting errors for Tafel slopes are under 2×10^{-3} V dec^{-1}) and water decomposition voltages – measured at 10 mA cm^{-2} and a 1000 mA cm^{-2} estimate.

Electrode	HER Tafel slope / mV dec^{-1}	OER Tafel slope / mV dec^{-1}	$U_{iR\text{-free}}$ @ 10 mA cm^{-2} / V	$U_{iR\text{-free}}$ @ 1000 mA cm^{-2} / V (estimate)
Ni-poly	−0.065	0.055	1.81	2.05
Rh@Ni-poly (10 seconds)	−0.075	0.068	1.66	1.95
Rh@Ni-poly (30 seconds)	−0.067	0.076	1.66	1.95
Pt-poly (RF = 5)	−0.100	0.152	1.87	2.37
Pt-poly (RF = 20)	−0.093	0.175	1.85	2.39

3.3. Electrocatalysis of HOR and ORR

After analyzing alkaline water electrolysis reactions, we turn to HOR and ORR – the key reactions in fuel cell technologies. HOR was measured in H_2-saturated 0.1 mol dm^{-3} at 10 mV s^{-1}, like in [50]. As the measurements were not fully stationary, some (pseudo)capacitive contributions are visible due to the H_{UPD} process. On the other hand, we wanted to avoid extensive Rh oxide formation, so we restricted voltammetric measurements to potentials beyond H_{UPD} peaks (i.e., double-layer region) where the capacitive response is the lowest. HOR was measured for Rh-modified Ni-poly electrode upon 30 s of exchange, directly after the replacement (**Figure 4**, a) and after prolonged cycling to 1.2 V *vs*. RHE (allowed to rest at 0 V vs. RHE for 10 min after cycling, **Figure 4** b). In both cases, diffusion limitations are reached, which can be seen from the equidistant diffusion currents and the Levich plot (**Figure 4**, d). However, in both cases diffusion currents are lower compared to the Pt-poly electrode and Pt/C-modified RDE from

Ref. [50]. Kinetic currents (j_k) evaluated at 0.05 V vs. RHE point that j_k for as-deposited Rh-modified electrode amounts 1.58 mA cm^{-2}, while after cycling it increases slightly to 1.75 mA cm^{-2}. Still, this is one order of magnitude lower compared to Pt-poly (RF = 20) where j_k was found to be 17.7 mA cm^{-2}. We note that Ni-poly does not have HOR activity [51], thus, the observed activity is solely due to the Rh phase. Previously, Rh-Ni alloys have been tested for HOR activity [51], and it was found that Rh-Ni alloys display composition-dependent activity, while the most active composition is $Ni_{89}Rh_{11}$ [51]. Interestingly, in that study as well diffusion-limiting currents commonly found for Pt electrodes were not reached on Rh-Ni alloy electrodes, and the diffusion currents we find here fall in the range of the ones reported in Ref. [51], where they have been measured under fully stationary conditions. Obviously, in contrast to HER, the HOR performance of Rh-modified electrodes is not as good and the electrodes perform not as well as platinum, despite tremendous activity improvements with respect to pure Ni-poly, which is not HOR active at all.

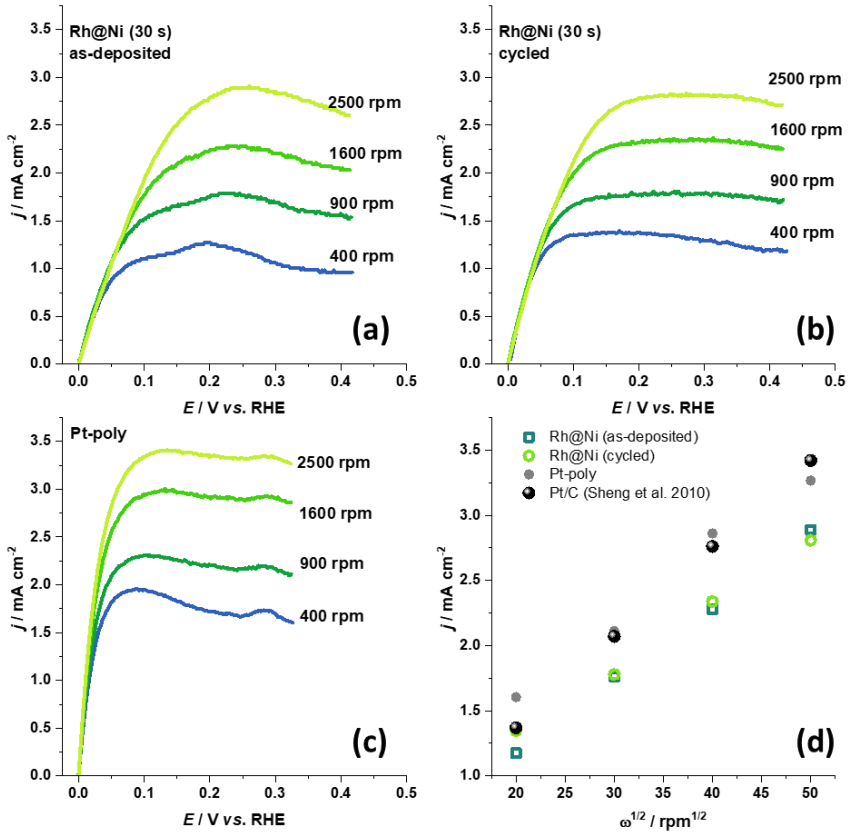

Figure 4. HOR polarization curves in alkaline media (H_2-saturated 0.1 mol dm^{-3} KOH, weep rate 10 mV s^{-1}) of (a) as deposited Rh-modified Ni-poly (30 s exchange), (b) extensively cycled Rh-modified Ni-poly electrode, (c) Pt-poly electrode, and (d) Levich plot (E = 0.3 V *vs*. RHE) for these three electrodes, including the reference values from Ref. [50] (done with Pt/C-modified RDE under identical experimental conditions as here).

Next, we study ORR on Rh-modified Ni-poly (**Figure 5**, a) and compare ORR performance to the Pt-poly electrode (RF = 20). Although in this work we have not prepared very smooth Ni-poly and its surface is rough, the RF is lower compared to the used Pt-poly benchmark where also small Pt particles are seen, being formed during the platinization (**Figure 5**, inset 3D SEM images). Higher RF of Pt-poly is also confirmed by a larger blank cyclic voltammogram compared to that of Rh-modified Ni-poly (**Figure 5**,

a and d). In the case of Pt-poly, full diffusion limitations corresponding to the $4e^-$ reduction of O_2 are reached. Moreover, there is a relatively small hysteresis between anodic and cathodic scan which is approximately 35 mV wide at the half-wave potential. ORR onset potential for Pt-poly was found to be close to 1.0 V vs. RHE. On the other hand, Rh-modified Ni-poly shows lower ORR onset potential (0.86 V vs. RHE), and much wider hysteresis between anodic and cathodic scans, amounting to 104 mV at the half-wave potential. In the case of Pt-poly, we have previously discussed how the effects of potential scan rate affect the hysteresis and ascribed its width to the slow Pt-oxide reduction under different potentiodynamic conditions [52]. Thus, when this knowledge is combined with the slow reduction of Rh-oxide discussed before (see **Figure 1**, b), larger hysteresis width in the case of Rh-modified Ni-poly, compared to Pt-poly, can be ascribed to hardly reducible Rh-oxides being formed on the electrode surface.

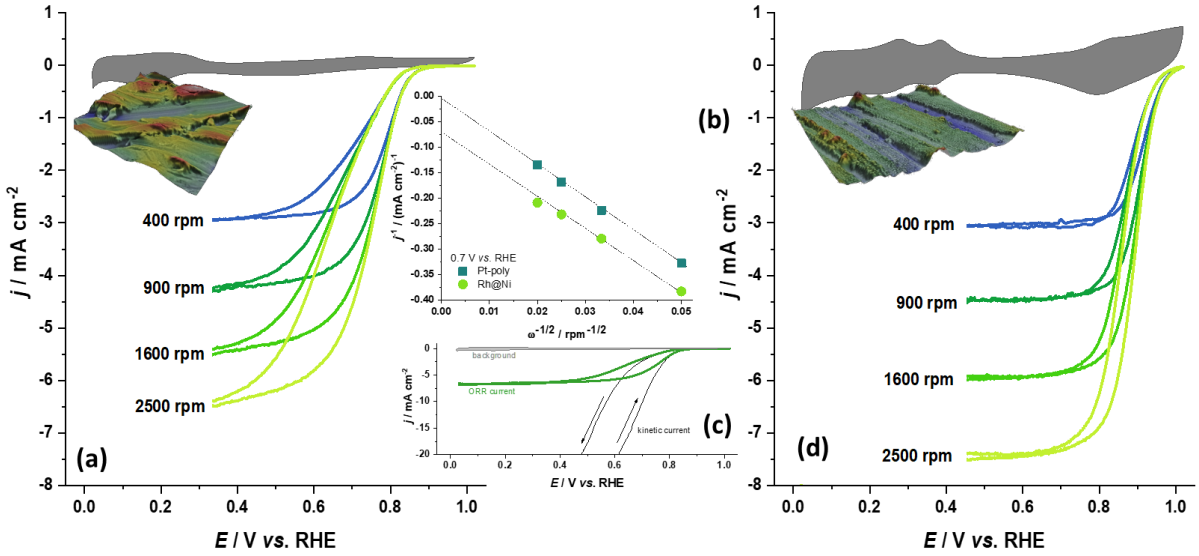

Figure 5. (a) Background-corrected ORR polarization curves and the blank cyclic voltammogram of Rh-modified Ni-poly electrode (30 s of exchange, O_2-saturated 0.1 mol dm^{-3} KOH, 20 mV s^{-1}, inset shows 3D reconstructed SEM image at ×10,000 magnification), (b) Koutecky-Levich plot for Pt-poly and Rh-modified Ni-poly electrode (at 0.5 V vs. RHE), (c) ORR polarization curve and calculated kinetic currents for ORR on Rh-modified Ni-poly, (d) background-corrected ORR polarization curves and the blank cyclic voltammogram of Pt-poly electrode (RF = 20, 30 s of exchange, 20 mV s^{-1}, inset shows 3D reconstructed SEM image at ×10,000 magnification).

We note that the relatively high ORR activity of the Rh-modified Ni-poly electrode is primarily due to the presence of Rh as the Ni-poly electrode has very poor ORR activity which is largely affected by the state of the surface, that is, the presence of Ni-oxide species. Moreover, the oxidation of Ni-poly surface in alkaline media leads to reduced selectivity of O_2 reduction and large amounts of peroxide formed [53]. Here, on the contrary, using the Koutecky-Levich (K-L) analysis [54], we found that ORR on the Rh-modified Ni-poly surface follows the $4e^-$ ORR path in the entire potential window where ORR was investigated (**Figure 5**, b). On the other hand, using the K-L analysis we have found that kinetic ORR currents (j_k) have finite values in the entire ORR potential window investigated, which were only a few times higher than limiting diffusion currents (j_d). Thus, using the K-L equation:

$$\frac{1}{j(E)} = \frac{1}{j_k(E)} + \frac{1}{j_d} \qquad (5)$$

we have evaluated j_k in the entire potential range studied here (**Figure 5**, c) and found it reaches up to 30±2 mA cm^{-2} (geometric) at 0.35 V vs. RHE. Error is associated with uncertainties due to the noise in limiting currents under diffusion conditions. Further, we have performed Tafel analysis on such reconstructed mass transfer-corrected kinetic currents and found that in the anodic scan, there is a continuous change of Tafel slope from low to high values. However, in the cathodic scan, the regions of different Tafel slopes were better separated, revealing the low Tafel slope region (−(67±2) mV dec^{-1}, from 0.85 to 0.81 V vs. RHE), medium Tafel slope (−(105±3) mV dec^{-1}, from 0.80 to 0.75 V vs. RHE), and high Tafel slope (−(217±2) mV dec^{-1}, down to 0.52 V vs. RHE). This behavior is similar to that of Pt revealed by using single submicrometer Pt particles [55], showing three ranges with different ORR Tafel slopes (−60, −105, and −240 mV dec^{-1}). Such behavior has been explained by the potential-dependent change in the oxide coverage and possible change of the ORR rate-determining step at high ORR overvoltages [55].

Based on the results presented so far, the effects of Rh oxide(s) on the catalytic performance of Rh-modified Ni-poly are very prominent. These are seen in HER catalysis as well as ORR catalysis, while the nature of the oxides present on the surface is crucial for OER catalysis. Based on Ref. [44], Rh forms two high-valence oxides at high potentials, Rh_2O_3 (above 0.9 V, orthorhombic phase), and RhO_2 (above 1.75 V, tetragonal phase). These thermodynamic data should be complemented by kinetic data for oxide formation and especially reduction, which is evidently very slow, and significantly impacts the ORR kinetics and the hysteresis between anodic and cathodic scans. Moreover, recently, the formation of Rh_2O_3 and RhO_2 was observed even during the electrodeposition of Rh-Ni alloys, while the oxides remained present during extended cycling in the HOR potential region (in alkaline media) [51]. Based on the DFT calculations we have performed on bulk Rh_2O_3 and RhO_2 (**Figure 6**), Rh_2O_3 is a semiconductor, with a bandgap of 0.51 eV. This bandgap is underestimated due to the methodology used, while a previous DFT+*U* study (*U* = 3.5 eV) indicated a bandgap of 1.14 eV [56]. Moreover, experimentally it was found that Rh_2O_3 has a direct band gap of 3.4 eV and an indirect band gap of 1.22 eV. On the other hand, higher-valence oxide, RhO_2, is a conductor (**Figure 6**). Thus, we believe that under ORR conditions, the Rh phase of the Rh-modified Ni-poly is converted to semiconducting Rh_2O_3, which impedes ORR. Additionally, the Rh surface is highly oxophilic leading to its low predicted ORR activity [25]. As Rh_2O_3 is reduced very slowly, it is also likely to be present to a low extent under the HOR condition, also impeding the rate of this reaction.

Under negative potentials corresponding to HER, Rh_2O_3 gets more reduced, but the negative impact of surface oxidation on the HER activity also suggests that the semiconducting oxide phase could be partially present even at very negative potentials, despite only metallic phase being thermodynamically stable under such conditions [44]. This is justified by the more pronounced (negative) impact of surface oxidation on the surface with a higher Rh content (**Figure 2**, middle versus bottom row). On the other hand, RhO_2, which is stable under high potential, is likely to be present during OER. This oxide is formed by the oxidation of Rh_2O_3 which means that the Rh phase converts from semiconducting to metallic one. Thus, OER activity is not impeded, while the OER activity of RhO_2 is expected to be very high [57]. In this way, by modifying the Ni-poly surface with Rh, high HER and OER activities were obtained, while the same surface underperforms in HOR and ORR compared to Pt-poly.

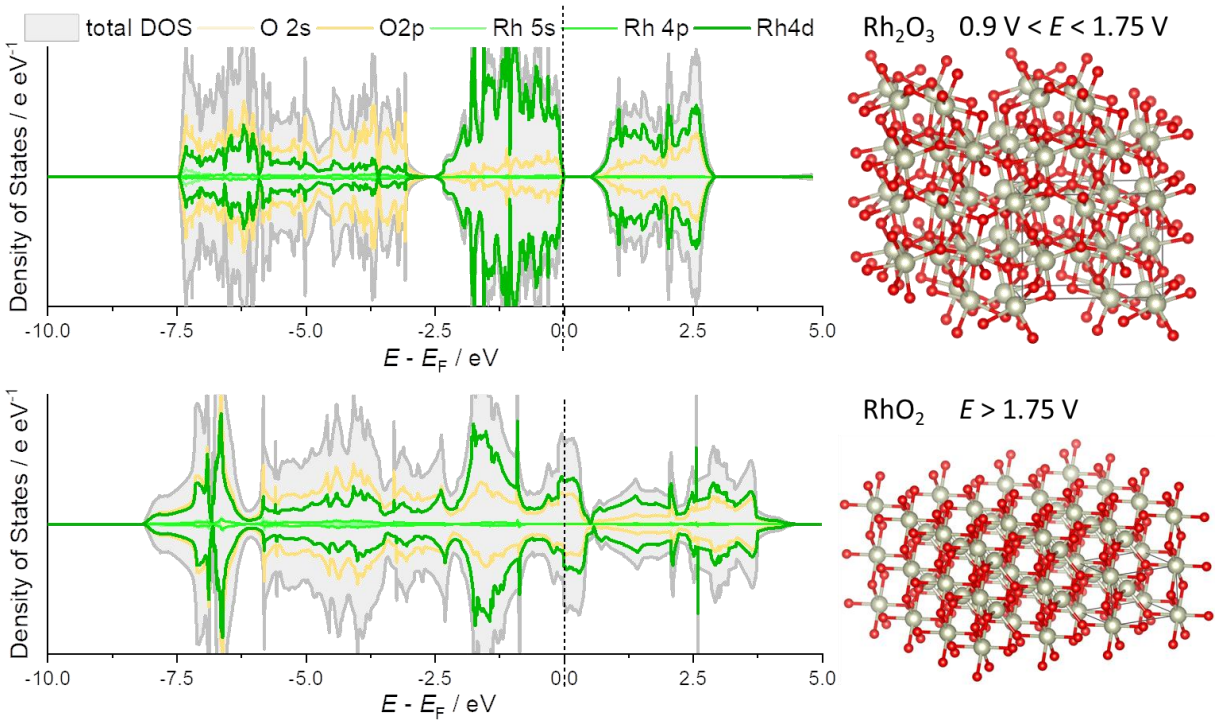

Figure 6. Densities of States and crystal structure of orthorhombic Rh_2O_3, stable between 0.9 and 1.75 V vs. RHE (top row), and tetragonal RhO_2, stable above 1.75 V vs. RHE (bottom row).

Finally, considering the use of Rh in electrocatalysis, the main obstacle is its price. Rh is one of the most expensive noble metals, with a price of 130.3 EUR *per* gram (after even five successive depreciations within the last year [27]). This is much higher compared to Pt (29.3 EUR *per* gram), but less than iridium (148.9 EUR *per* gram) which is practically the only metal that is considered viable for PEM electrolysis anodes [58,59]. Moreover, based on preliminary testing, the rapid galvanic displacement using platinum solution under identical conditions does not lead to appreciable catalytic activity improvements comparable to the case of Ni modification by Rh. Thus, optimizing Rh deposition to minimize its usage and restricting to the surface modifications of low-cost substrates could be a plausible route for designing novel high-performance alkaline electrolysis catalysts leading to tremendous energy saving. These savings could even justify the use of more expensive metals. However, in order to make more concrete conclusions regarding this possibility, it is necessary to consider factors beyond electrocatalytic performance.

4. Conclusions

In the present work, we have demonstrated the high HER and OER activities of Rh-modified polycrystalline Ni electrodes in alkaline media. Based on the evaluated HER and OER overpotentials and also low values of Tafel slopes for these two reactions, it is estimated that Rh-modified Ni electrodes ensure alkaline electrolysis at high current densities (1 A cm^{-2}) at a voltage below 2 V. Moreover, in contrast to pure Ni, the Rh-modified electrode shows appreciable HOR activity and much improved ORR activity. Nevertheless, their HOR and ORR performance is lower compared to polycrystalline platinum. When studying each of these reactions, the effects of surface oxidation have shown to be very important. Namely, anodically formed Rh oxides are very difficult to reduce, affecting HER/HOR and, particularly,

ORR. Such effects can be understood on the basis of the semiconducting nature of Rh_2O_3 formed at lower potentials, impeding ORR and partially also HOR. Moreover, when the electrode is intentionally oxidized, HER activity is also affected, being reduced when compared to freshly prepared Rh-modified electrodes. On the other hand, OER takes place at higher potentials where RhO_2 is formed, which is conductive and does not affect electron transfer. Overall, the presented results place facile galvanic displacement of Ni with Rh as a suitable route for engineering highly active water splitting electrocatalysts for alkaline electrolysis. This conclusion is also supported by a very low price penalty introduced by surface modification with Rh and significantly reduced Rh price in the last 12 months, currently below the price of iridium.

Acknowledgment

A.Z.J. and I.A.P. acknowledge the support provided by the Serbian Ministry of Science, Technological Development, and Innovation (451-03-47/2023-01/200146). S.V.M. and I.A.P. acknowledge the support of the Serbian Academy of Sciences and Arts, provided through the project F-190: Electrocatalysis in contemporary processes of energy conversion. The computations and data handling were enabled by resources provided by the National Academic Infrastructure for Supercomputing in Sweden (NAISS) at the NSC center of Linköping University, partially funded by the Swedish Research Council through grant agreement no. 2018-05973.

References

[1] I.A. Pašti, E. Fako, A.S. Dobrota, N. López, N. V Skorodumova, S. V Mentus, Atomically Thin Metal Films on Foreign Substrates: From Lattice Mismatch to Electrocatalytic Activity, ACS Catal. 9 (2019) 3467–3481. doi:10.1021/acscatal.8b04236.

[2] R. Schlögl, Sustainable Energy Systems: The Strategic Role of Chemical Energy Conversion, Top. Catal. 2016 598. 59 (2016) 772–786. doi:10.1007/S11244-016-0551-9.

[3] J.O. Abe, A.P.I. Popoola, E. Ajenifuja, O.M. Popoola, Hydrogen energy, economy and storage: Review and recommendation, Int. J. Hydrogen Energy. 44 (2019) 15072–15086. doi:10.1016/J.IJHYDENE.2019.04.068.

[4] M. Yue, H. Lambert, E. Pahon, R. Roche, S. Jemei, D. Hissel, Hydrogen energy systems: A critical review of technologies, applications, trends and challenges, Renew. Sustain. Energy Rev. 146 (2021) 111180. doi:https://doi.org/10.1016/j.rser.2021.111180.

[5] M. Nasser, T.F. Megahed, S. Ookawara, H. Hassan, A review of water electrolysis–based systems for hydrogen production using hybrid/solar/wind energy systems, Environ. Sci. Pollut. Res. 29, 86994–87018 (2022). doi:10.1007/S11356-022-23323-Y.

[6] M. Chatenet, B.G. Pollet, D.R. Dekel, F. Dionigi, J. Deseure, P. Millet, R.D. Braatz, M.Z. Bazant, M. Eikerling, I. Staffell, P. Balcombe, Y. Shao-Horn, H. Schäfer, Water electrolysis: from textbook knowledge to the latest scientific strategies and industrial developments, Chem. Soc. Rev. 51 (2022) 4583–4762. doi:10.1039/D0CS01079K.

[7] A.J. Shih, M.C.O. Monteiro, F. Dattila, D. Pavesi, M. Philips, A.H.M. da Silva, R.E. Vos, K. Ojha, S. Park, O. van der Heijden, G. Marcandalli, A. Goyal, M. Villalba, X. Chen, G.T.K.K. Gunasooriya, I. McCrum, R. Mom, N. López, M.T.M. Koper, Water electrolysis, Nat. Rev. Methods Primers 2, (2022) 1–19. doi:10.1038/s43586-022-00164-0.

[8] S. Shiva Kumar, V. Himabindu, Hydrogen production by PEM water electrolysis – A review, Mater. Sci. Energy Technol. 2 (2019) 442–454. doi:10.1016/J.MSET.2019.03.002.

[9] V.A. Panchenko, Y. V. Daus, A.A. Kovalev, I. V. Yudaev, Y. V. Litti, Prospects for the production of green

hydrogen: Review of countries with high potential, Int. J. Hydrogen Energy. 48 (2023) 4551–4571. doi:10.1016/J.IJHYDENE.2022.10.084.

[10] L. Fan, Z. Tu, S.H. Chan, Recent development of hydrogen and fuel cell technologies: A review, Energy Reports. 7 (2021) 8421–8446. doi:10.1016/J.EGYR.2021.08.003.

[11] A. Kirubakaran, S. Jain, R.K. Nema, A review on fuel cell technologies and power electronic interface, Renew. Sustain. Energy Rev. 13 (2009) 2430–2440. doi:10.1016/J.RSER.2009.04.004.

[12] N. Sazali, W.N.W. Salleh, A.S. Jamaludin, M.N.M. Razali, New Perspectives on Fuel Cell Technology: A Brief Review, Membr. 2020, Vol. 10, Page 99. doi:10.3390/MEMBRANES10050099.

[13] X. Hu, X. Tian, Y.W. Lin, Z. Wang, Nickel foam and stainless steel mesh as electrocatalysts for hydrogen evolution reaction, oxygen evolution reaction and overall water splitting in alkaline media, RSC Adv. 9 (2019) 31563–31571. doi:10.1039/C9RA07258F.

[14] M.A. McArthur, L. Jorge, S. Coulombe, S. Omanovic, Synthesis and characterization of 3D Ni nanoparticle/carbon nanotube cathodes for hydrogen evolution in alkaline electrolyte, J. Power Sources. 266 (2014) 365–373. doi:10.1016/J.JPOWSOUR.2014.05.036.

[15] S.H. Ahn, S.J. Hwang, S.J. Yoo, I. Choi, H.J. Kim, J.H. Jang, S.W. Nam, T.H. Lim, T. Lim, S.K. Kim, J.J. Kim, Electrodeposited Ni dendrites with high activity and durability for hydrogen evolution reaction in alkaline water electrolysis, J. Mater. Chem. 22 (2012) 15153–15159. doi:10.1039/C2JM31439H.

[16] J.R. Kitchin, J.K. Nørskov, M.A. Barteau, J.G. Chen, Modification of the surface electronic and chemical properties of Pt(111) by subsurface 3d transition metals, J. Chem. Phys. 120 (2004) 10240–10246. doi:10.1063/1.1737365.

[17] Q. Jia, W. Liang, M.K. Bates, P. Mani, W. Lee, S. Mukerjee, Activity descriptor identification for oxygen reduction on platinum-based bimetallic nanoparticles: In situ observation of the linear composition-strain-activity relationship, ACS Nano. 9 (2015) 387–400. doi:10.1021/NN506721F

[18] I.A. Raj, K.I. Vasu, Transition metal-based hydrogen electrodes in alkaline solution - electrocatalysis on nickel based binary alloy coatings, J. Appl. Electrochem. 20 (1990) 32–38. doi:10.1007/BF01012468

[19] R. Solmaz, A. Döner, G. Kardaş, The stability of hydrogen evolution activity and corrosion behavior of NiCu coatings with long-term electrolysis in alkaline solution, Int. J. Hydrogen Energy. 34 (2009) 2089–2094. doi:10.1016/J.IJHYDENE.2009.01.007.

[20] I. Herraiz-Cardona, C. González-Buch, C. Valero-Vidal, E. Ortega, V. Pérez-Herranz, Co-modification of Ni-based type Raney electrodeposits for hydrogen evolution reaction in alkaline media, J. Power Sources. 240 (2013) 698–704. doi:10.1016/J.JPOWSOUR.2013.05.041.

[21] R. Subbaraman, D. Tripkovic, K.C. Chang, D. Strmcnik, A.P. Paulikas, P. Hirunsit, M. Chan, J. Greeley, V. Stamenkovic, N.M. Markovic, Trends in activity for the water electrolyser reactions on 3d M(Ni,Co,Fe,Mn) hydr(oxy)oxide catalysts, Nat. Mater. 11 (2012) 550–557. doi:10.1038/nmat3313.

[22] S.J. Gutić, A.S. Dobrota, M. Leetmaa, N. V. Skorodumova, S. V. Mentus, I.A. Pašti, Improved catalysts for hydrogen evolution reaction in alkaline solutions through the electrochemical formation of nickel-reduced graphene oxide interface, Phys. Chem. Chem. Phys. 19 (2017) 13281–13293. doi:10.1039/C7CP01237C.

[23] D. Chanda, J. Hnát, A.S. Dobrota, I.A. Pa?ti, M. Paidar, K. Bouzek, The effect of surface modification by reduced graphene oxide on the electrocatalytic activity of nickel towards the hydrogen evolution reaction, Phys. Chem. Chem. Phys. 17 (2015) 26864–26874. doi:10.1039/c5cp04238k.

[24] J.K. Nørskov, T. Bligaard, A. Logadottir, J.R. Kitchin, J.G. Chen, S. Pandelov, U. Stimming, Trends in the Exchange Current for Hydrogen Evolution, J. Electrochem. Soc. 152 (2005) J23. doi:10.1149/1.1856988/XML.

[25] J.K. Nørskov, J. Rossmeisl, A. Logadottir, L. Lindqvist, J.R. Kitchin, T. Bligaard, H. Jónsson, Origin of the Overpotential for Oxygen Reduction at a Fuel-Cell Cathode, J. Phys. Chem. B. 108 (2004) 17886–17892. doi:10.1021/JP047349J.

[26] C.C.L. McCrory, S. Jung, I.M. Ferrer, S.M. Chatman, J.C. Peters, T.F. Jaramillo, Benchmarking Hydrogen Evolving Reaction and Oxygen Evolving Reaction Electrocatalysts for Solar Water Splitting Devices, J. Am. Chem. Soc. 137 (2015) 4347–4357. doi:10.1021/JA510442P

[27] Metals prices | Umicore Precious Metals Management, (n.d.). https://pmm.umicore.com/en/prices/ (accessed August 2nd, 2023).

[28] Y. Yuan, N. Yan, P.J. Dyson, Advances in the rational design of rhodium nanoparticle catalysts: Control via manipulation of the nanoparticle core and stabilizer, ACS Catal. 2 (2012) 1057–1069. doi:10.1021/CS300142U

[29] M.K. Kundu, R. Mishra, T. Bhowmik, S. Barman, Rhodium metal–rhodium oxide (Rh–Rh2O3) nanostructures with Pt-like or better activity towards hydrogen evolution and oxidation reactions (HER, HOR) in acid and base: correlating its HOR/HER activity with hydrogen binding energy and oxophilicity of the catalyst, J. Mater. Chem. A. 6 (2018) 23531–23541. doi:10.1039/C8TA07028H.

[30] M.A. Montero, M.R. Gennero De Chialvo, A.C. Chialvo, Kinetics of the hydrogen oxidation reaction on nanostructured rhodium electrodes in alkaline solution, J. Power Sources. 283 (2015) 181–186. doi:10.1016/J.JPOWSOUR.2015.02.133.

[31] P. Benito, V. Dal Santo, V. De Grandi, M. Marelli, G. Fornasari, R. Psaro, A. Vaccari, Coprecipitation versus chemical vapour deposition to prepare Rh/Ni bimetallic catalysts, Appl. Catal. B Environ. 179 (2015) 150–159. doi:10.1016/J.APCATB.2015.05.016.

[32] N. Schiaroli, C. Lucarelli, G. Sanghez de Luna, G. Fornasari, A. Vaccari, Ni-based catalysts to produce synthesis gas by combined reforming of clean biogas, Appl. Catal. A Gen. 582 (2019) 117087. doi:10.1016/J.APCATA.2019.05.021.

[33] A.Z. Jovanović, L. Bijelić, A.S. Dobrota, N. V. Skorodumova, S. V. Mentus, I.A. Pašti, Enhancement of hydrogen evolution reaction kinetics in alkaline media by fast galvanic displacement of nickel with rhodium – From smooth surfaces to electrodeposited nickel foams, Electrochim. Acta. 414 (2022) 140214. doi:10.1016/J.ELECTACTA.2022.140214.

[34] B. Nedić Vasiljević, A.Z. Jovanović, S. V. Mentus, N. V. Skorodumova, I.A. Pašti, Galvanic displacement of Co with Rh boosts hydrogen and oxygen evolution reactions in alkaline media, J. Solid State Electrochem. 27 (2023) 1877–1887. doi:10.1007/S10008-023-05374-4

[35] S. Trasatti, O.A. Petrii, International Union of Pure and Applied Chemistry Physical Chemistry Division Commission on Electrochemistry: Real Surface Area Measurements in Electrochemistry, Pure Appl. Chem. 63 (1991) 711–734. doi:10.1351/PAC199163050711

[36] I.A. Pašti, N.M. Gavrilov, S. V Mentus, Electrocatalytic behavior of Pt/WO_3 composite layers formed potentiodynamically on tungsten surfaces, Int. J. Electrochem. Sci. 12 (2017) 5772–5791. doi:10.20964/2017.06.80.

[37] G. Kresse, J. Furthmüller, Efficiency of ab-initio total energy calculations for metals and semiconductors using a plane-wave basis set, Comput. Mater. Sci. 6 (1996) 15–50. doi:10.1016/0927-0256(96)00008-0.

[38] G. Kresse, J. Furthmüller, Efficient iterative schemes for *ab initio* total-energy calculations using a plane-wave basis set, Phys. Rev. B. 54 (1996) 11169. doi:10.1103/PhysRevB.54.11169.

[39] J.P. Perdew, K. Burke, M. Ernzerhof, Generalized Gradient Approximation Made Simple, Phys. Rev. Lett. 77 (1996) 3865. doi:10.1103/PhysRevLett.77.3865.

[40] P.E. Blöchl, Projector augmented-wave method, Phys. Rev. B. 50 (1994) 17953–17979. doi:10.1103/PhysRevB.50.17953.

[41] P.E. Blöchl, O. Jepsen, O.K. Andersen, Improved tetrahedron method for Brillouin-zone integrations, Phys. Rev. B. 49 (1994) 16223. doi:10.1103/PhysRevB.49.16223.

[42] M. Łukaszewski, H. Siwek, A. Czerwiński, Electrochemical behavior of thin polycrystalline rhodium layers studied by cyclic voltammetry and quartz crystal microbalance, Electrochim. Acta. 52 (2007) 4560–4565. doi:10.1016/J.ELECTACTA.2006.12.066.

[43] E.F. Holby, J. Greeley, D. Morgan, Thermodynamics and hysteresis of oxide formation and removal on platinum (111) surfaces, J. Phys. Chem. C. 116 (2012) 9942–9946. doi:10.1021/JP210805Z/SUPPL_FILE/JP210805Z_SI_002

[44] M. Schellenbach, O. Kasian, M. Ledendecker, F.D. Speck, A.M. Mingers, K.J.J. Mayrhofer, S. Cherevko, The Electrochemical Dissolution of Noble Metals in Alkaline Media, Electrocatalysis. 9 (2018) 153–161. doi:10.1007/S12678-017-0438-Y

[45] N. Danilovic, R. Subbaraman, D. Strmcnik, K.C. Chang, A.P. Paulikas, V.R. Stamenkovic, N.M. Markovic, Enhancing the Alkaline Hydrogen Evolution Reaction Activity through the Bifunctionality of Ni(OH)2/Metal Catalysts, Angew. Chemie Int. Ed. 51 (2012) 12495–12498. doi:10.1002/ANIE.201204842.

[46] R. Subbaraman, D. Tripkovic, D. Strmcnik, K.C. Chang, M. Uchimura, A.P. Paulikas, V. Stamenkovic, N.M. Markovic, Enhancing hydrogen evolution activity in water splitting by tailoring Li+-Ni(OH)2-Pt interfaces, Science 334 (2011) 1256–1260. doi:10.1126/SCIENCE.1211934

[47] Neumüller, D.; Rafailović, L.D.; Jovanović, A.Z.; Skorodumova, N.V.; Pašti, I.A.; Lassnig, A.; Griesser, T.; Gammer, C.; Eckert, J. Hydrogen Evolution Reaction on Ultra-Smooth Sputtered Nanocrystalline Ni Thin Films in Alkaline Media—From Intrinsic Activity to the Effects of Surface Oxidation. Nanomaterials 2023, 13, 2085. https://doi.org/10.3390/nano13142085

[48] P.K. Wrona, A. Lasia, M. Lessard, H. Ménard, Kinetics of the hydrogen evolution reaction on a rhodium electrode, Electrochim. Acta. 37 (1992) 1283–1294. doi:10.1016/0013-4686(92)85069-W.

[49] M. Plevová, J. Hnát, K. Bouzek, Electrocatalysts for the oxygen evolution reaction in alkaline and neutral media. A comparative review, J. Power Sources. 507 (2021) 230072. doi:10.1016/J.JPOWSOUR.2021.230072.

[50] W. Sheng, H.A. Gasteiger, Y. Shao-Horn, Hydrogen Oxidation and Evolution Reaction Kinetics on Platinum: Acid vs Alkaline Electrolytes, J. Electrochem. Soc. 157 (2010) B1529. doi:10.1149/1.3483106/XML.

[51] D.S. Tran, H. Park, H. Kim, S.K. Kim, Electrodeposited NiRh alloy as an efficient low-precious metal catalyst for alkaline hydrogen oxidation reaction, Int. J. Energy Res. 45 (2021) 5325–5336. doi:10.1002/ER.6155.

[52] I.A. Pasti, N.M. Gavrilov, S. V. Mentus, Potentiodynamic Investigation of Oxygen Reduction Reaction on Polycrystalline Platinum Surface in Acidic Solutions: the Effect of the Polarization Rate on the Kinetic Parameters, Int. J. Electrochem. Sci. 7 (2012) 11076–11090. doi:10.1016/S1452-3981(23)16928-8.

[53] V.S. Bagotzky, N.A. Shumilova, G.P. Samoilov, E.I. Khrushcheva, Electrochemical oxygen reduction on nickel electrodes in alkaline solutions—II, Electrochim. Acta. 17 (1972) 1625–1635. doi:10.1016/0013-4686(72)85053-9.

[54] A.J. Bard, L.R. Faulkner, Electrochemical Methods: Fundamentals and Applications, 2nd Edition, John Wiley \& Sons, Incorporated, 2000.

[55] S. Chen, A. Kucernak, Electrocatalysis under Conditions of High Mass Transport Rate: Oxygen Reduction on Single Submicrometer-Sized Pt Particles Supported on Carbon, J. Phys. Chem. B. 108 (2004) 3262–3276. doi:10.1021/JP036831J.

[56] Y.D. Scherson, S.J. Aboud, J. Wilcox, B.J. Cantwell, Surface structure and reactivity of rhodium oxide, J. Phys. Chem. C. 115 (2011) 11036–11044. doi:10.1021/JP110998E

[57] E. Fabbri, A. Habereder, K. Waltar, R. Kötz, T.J. Schmidt, Developments and perspectives of oxide-based catalysts for the oxygen evolution reaction, Catal. Sci. Technol. 4 (2014) 3800–3821. doi:10.1039/C4CY00669K.

[58] M. Bele, G.K. Podboršek, A. Lončar, P. Jovanovič, A. Hrnjić, Ž. Marinko, J. Kovač, A.K. Surca, A.R. Kamšek, G. Dražić, N. Hodnik, L. Suhadolnik, " Nano Lab " Advanced Characterization Platform for Studying Electrocatalytic Iridium Nanoparticles Dispersed on TiOxNy Supports Prepared on Ti Transmission Electron Microscopy Grids , ACS Appl. Nano Mater. 6 (2023) 10421–10430. doi:10.1021/ACSANM.3C01368

[59] A. Lončar, P. Jovanovič, N. Hodnik, M. Gaberšček, Determination of the Electroactive Surface Area of Supported Ir-Based Oxygen Evolution Catalysts by Impedance Spectroscopy: Observed Anomalies with Respect to Catalyst Loading, J. Electrochem. Soc. 170 (2023) 044504. doi:10.1149/1945-7111/ACCAAD.